Shear strength of a silt at various oil/water contents

Authors: Jiaren Yu, Chao Zhou, and Qingyi Mu*

*Corresponding author

Abstract

It is important to understand the shear behaviour of oil-contaminated soils in many geotechnical problems, such as the analysis of pipelines and storage tanks affected by oil leakage. In this study, the shear behaviour of a silt permeated with silicone oil/water (denoted by OS and WS, respectively) was investigated through direct shear tests. The residual shear strength was measured at various degrees of liquid saturation (65% to 100%) and net normal stresses (50 to 400 kPa). The oil and water retention curves were measured and used to explain the shear behaviour. The results show that the residual friction angle of OS is 30% larger than that of WS. This is likely because OS and WS show aggregated and matrix structures, respectively, as evidenced by the Scanning Electron Microscope (SEM) test. The former structure includes more particle contacts than the latter one. These structural differences can be attributed to varying fluid properties, such as wettability, viscosity, and dielectric constant. When the volumetric degree of water saturation decreases, the total cohesion of WS increases substantially because of the strengthening effects of air-water interfaces on the soil skeleton. In contrast, the degree of oil saturation has minuscule effects on these variables, mainly because OS has a low oil retention ability and the air-oil suction remains very low (i.e., less than 2 kPa) during the desaturation process.

Keywords: Shear strength; Oil-contaminated soil; Unsaturated soil; Soil water retention curve

NOTATION

a, n, m	soil parameters in the VG model (van Genuchten, 1980)
β	scaling factor that equals the ratio of interfacial tensions
c_{brine}	concentration of NaCl brine (g/g)
c_t	total cohesion
e_{io}	void ratio of oil-filled specimen
e_{iw}	void ratio of water-filled specimen
G_{ker}	the ratio of the unit weight of kerosene to that of water
LL_{DW}	liquid limit of soil with deionized water
LL_{brine}	liquid limit of soil with 2-M NaCl brine
LL_{ker}	liquid limit of soil with kerosene
S_r	volumetric degree of liquid saturation
S_o	volumetric degree of oil saturation
S_w	volumetric degree of water saturation
s	matric suction
s_{aw}	suction produced by the air-water interface
s_{ao}	suction produced by the air-oil interface
T_{al}	interfacial tensions of air-scaled liquid
T_{aw}	interfacial tensions of air-water
T_{ao}	interfacial tensions of air-oil
u_a	pore air pressure
u_o	oil pressure
u_w	water pressure
σ	total normal stress
σ - u_a	net normal stress
τ_f	shear strength of soil
ϕ'	effective friction angle

1. Introduction

Oil contamination of the ground is a worldwide issue and its influence on soil behaviour should be evaluated in many geotechnical problems. For example, a huge amount of oil pipelines and storage tanks have been constructed around the world with the rising demand for energy (Al-Sanad et al., 1995; Khosravi et al., 2013; Nasr and Krishna Rao, 2016). During their lifetime, the surrounding soils are potentially subjected to oil contamination, which may affect the properties of soils and hence, the stability of pipelines and storage tanks. This has been confirmed by the physical model tests of Nasr

and Krishna Rao (2016) and Nasr (2013), who reported significant decreases in the lateral resistance of pile groups and the uplift resistance of single pile induced by oil contamination.

The stability of geo-structures is closely related to the shear behaviour of soils. To improve the analysis and design, the shear behaviour of oil-contaminated soils before and after the remediation should be evaluated (ur Rehman et al., 2023). In this area, previous researchers have carried out some experimental investigations. Their methodologies may be classified into two major types. In the first one, a given amount of oil is added to a soil specimen partially saturated with water, which results in a complicated four-phase material comprising solid particles, water, oil and air. By using this method, Kermani and Ebadi (2012) studied the influence of oil content on the shear behaviour of clay through direct shear tests. When the oil content increased from zero to 15% at a given water content (e.g., 9%), the friction angle increased by about 33%, and the cohesion decreased by about 80%. Ghadyani et al. (2019) tested a clay and observed an opposite trend. With an increase of oil content from zero to 9% at a given water content (e.g., 17%, 19% and 21%), the average friction angle decreased by about 37% while the average cohesion increased by about 38%. For the four-phase specimen, the interactions among air, oil, water, and particles develop contractile skins at the air-water, air-oil, and oil-water surfaces (Cui et al., 2003; Yu et al., 2022). Due to capillary effects, each contractile skin would contribute to the soil hardening through the surface tension. It is not easy to evaluate the effects of each contractive skin on the shear behaviour by directly testing oil-contaminated unsaturated soil, which is a four-phase material (air-oil-water-particle). This partially explains the discrepancies in the shear behaviour of oil-contaminated soils obtained in previous studies. Therefore, a simplified approach was adopted in most studies, in which the three-phase specimen (i.e., particle-oil-air mixture) was used.

By taking the second approach (tests on the three-phase specimen), the absence of water in the specimen eliminates the contractile skins of air-water and oil-water and makes it easy to interpret the oil effects from the viewpoint of unsaturated soil mechanics. Therefore, the effects of the contractile skin at the air-oil surface on the shear behaviour could be investigated. Al-Sanad et al. (1995) investigated the shear strength of sand at different oil contents through direct shear tests. When the oil content was increased from zero to 6%, there were clear reductions in both shear strength (up to 25%) and friction angle (up to 10^{o}). Similar strength weakening with increasing oil content was observed by other studies investigating sand (Puri, 2000; Shin and Das, 2001; Nasr, 2009 and 2013; Nasr and Krishna Rao, 2016) and clay (Jia et al., 2011; Khosravi et al., 2013; Nasehi et al., 2016; Safehian et al., 2018).

The effects of oil content on the shear behaviour of sand can probably be explained by the negative pore oil pressure and the capillary force occurring in the oil meniscus. The impact of oil on clay is more complicated than on sand due to the more active minerals in the former soil. Based on previous studies (Nasehi et al., 2016; Rajabi and Sharifipour, 2019; Izdebska-Mucha and Trzciński, 2021), the fabrics of clayey soils mixed with water and oil are also different due to the different interactions of clay minerals with water and oil. It is expected that the effects of oil content on the shear behaviour of clay are controlled by both suction and structure effects. On the one hand, several literatures indicated that suction or degree of saturation has a significant impact on shear strength, compressibility (Ijaz et al., 2022a), slope stability (Ijaz et al., 2022b) and hydraulic conductivity (Rehman et al., 2023). The effects of oil contamination on cohesion have not been concluded unanimously. The reported cohesion can increase, decrease or remain almost unchanged with increasing oil content (Khamehchiyan et al., 2007; Khosravi et al., 2013; Safehian et al., 2018). On the other hand, the impacts of oil on the shear

behaviour of clay and the subsequent alteration of soil structure have been found to be influenced by the properties of the organic fluid, such as viscosity and dielectric constant. A series of UC triaxial tests conducted by Ratnaweera and Meegoda (2006) has demonstrated a strong correlation between the shearing behaviour of contaminated soils and the viscosity of the pore fluid. Their findings indicate that as the fluid viscosity increases, the soil shear strength decreases, and the stress-strain behaviour exhibits softening tendencies. This phenomenon can be attributed to the hypothesis that an increase in pore fluid viscosity alters the properties of mineral-to-pore fluid contacts, leading to a softening of the stress-strain behaviour (Sherif and Burrous, 1969). Additionally, it is worth noting that soil with higher pore fluid viscosity tends to exhibit a more densely packed structure compared to the same soil with water as the pore fluid (Ratnaweera and Meegoda, 2006). In addition, Moore and Mitchell (1974) reported a significant dependence of kaolinite shear strength on the dielectric constant of the fluids. This trend was found to qualitatively align with variations in the attractive forces between clay particles, which are influenced by the fluid's dielectric constant.

Although previous studies have improved the understanding of oil contamination on the shear behaviour of soils, some research gaps in previous studies still need to be addressed. Firstly, oil contamination can affect soil behaviour via at least two mechanisms: alternation of microstructure (Nasehi et al., 2016; Rajabi and Sharifipour, 2019) and suction of air-oil interfaces (Cui et al., 2003; Goel and O'Carroll, 2011). So far, most studies focused on the former mechanism, while less attention was paid to the latter. Secondly, it is recognized that the behaviour of unsaturated soils is closely related to the liquid retention behaviour (Fredlund and Rahardjo, 1993; Ng and Menzies, 2007). The effects of oil retention ability on the shear behaviour of oil-contaminated soils have not been explored.

This study aims to investigate the shear strength of oil-contaminated soil at various oil contents.

To achieve this objective, a series of direct shear tests were carried out using silt at various degrees of silicone oil saturation. For comparison, the shear behaviour of this silt at various degrees of water saturation was also determined. The oil and water retention curves were measured to evaluate the suction ranges. In addition, the Scanning Electron Microscope (SEM of oil and water-permeated specimens were obtained to interpret their shear behaviour from a microscopic viewpoint. The methodology and results are presented in the following sections, where the abbreviations of OS and WS represent specimens permeated with oil and water, respectively. Note that the testing of the three-phase specimens (i.e., air-oil-particle and air-water-particle) may not reflect the real situation, as the oil-contaminated unsaturated soils have four phases (i.e., air-water-oil-particle). In future studies, some advanced apparatuses could be developed to independently control specimens' air, oil and water pressures. The effects of each liquid on the shear behaviour of oil-contaminated soil could be well identified and interpreted based on unsaturated soil mechanics.

2. Material and method

2.1. Test programme

Three series of tests were designed and carried out (see Table 1). Series I was designed to investigate the oil and water retention curves (ORC and WRC). Considering the degree of compaction required for our specimens, an appropriate gravimetric water content (8.4%) was selected as the initial water content after conducting several trial runs and became the reference of OS.

In the second and third series, the shear behaviour of OS and WS at various degrees of oil/water saturation was studied. Each series consists of sixteen specimens with consideration of four degrees of oil/water saturation, including 100%, 81%, 72% and 65%, denoted by S1, S2, S3 and S4. At each degree of saturation, four normal stresses were applied prior to shearing: 50, 100, 200 and 400 kPa (i.e., N50, N100, N200 and N400). Since the direct shear test is not suction controlled, the suction values of OS and WS cannot be accurately determined. They could only be estimated with the

assistance of ORC and WRC measured in Series I to qualitatively evaluate the unsaturation effects on soil shear behaviour. The study of WS serves as a benchmark for that of OS. The test specimens include water-filled or oil-filled CDG with high degrees of saturation (e.g., $S_r > 65\%$). This degree of saturation range is selected to avoid a wide suction range (i.e., from very dry to saturated conditions) (e.g., Sheng et al., 2011; Han and Vanapalli, 2016; Ng et al., 2017), which would influence the failure criteria of unsaturated soils fundamentally. For example, Ng et al. (2017) proved that the failure criteria of unsaturated soils cannot well capture the variation in the shear strength of unsaturated loess when the degree of water saturation is less than 15%.

To investigate the microstructures of OS and WS, SEM tests were carried out on the specimens OS-S3 and WS-S3. The results were used to interpret the influence of fluid type on the soil shear behaviour.

2.2. Test materials and specimen preparation

A completely decomposed granitic (CDG) soil, which falls into the category of silt (Hossain & Yin, 2010), was used in this study. The collected CDG soil was oven-dried and passed through a 2 mm sieve to remove the gravel-sized particles. As shown in Figure 2, the sand, silt and clay fractions of the used soil are 49.1%, 28.8% and 22.1%, respectively. The particle size distribution was measured following the procedures in ASTM D6913/D6913M-17 (ASTM 2017c) and ASTM D7928-17 (ASTM 2017d). The Atterberg limits test was conducted following ASTM D4318-17 (ASTM 2017a), and the liquid and plastic limits are 31.6% and 21.2%, respectively. Based on the compaction tests using the standard effort (ASTM, 2012), the optimum water content and maximum dry density are 13.4% and 1.84 g/cm^3. More details of the soil properties are given in Table 2.

Similar to many previous studies (Ye et al., 2012; Soga et al., 2003; Goel and O'Carroll, 2011), silicone oil was used for preparing OS because it is non-toxic, pure, and stable. Furthermore, silicone oil has similar dielectric permittivity and wettability to common NAPL contaminants, e.g., petroleum hydrocarbons and motor oil. These two physical properties of liquid play a crucial role in the liquid-

particle interaction (Mitchell and Soga, 2005). The silicone oil also has a low viscosity, so the duration of the ORC test can be shortened. More properties of the silicone oil are summarized in Table 3.

The static compaction method was used to prepare all specimens. The soil was first oven-dried and passed through a 2 mm sieve. For the measurement of ORC (series I), the oven-dried soil was mixed with oil to a gravimetric oil content of 8.4%, which is defined as the oil mass per unit mass of dry soil. The mixture was compacted into an oedometer ring with diameter and height equaling 60 mm and 20 mm, respectively. The initial dry density after compaction is 1.75 g/cm^3, which corresponds to 95% of the maximum dry density of water-filled CDG. Such a high degree of compaction is selected because it is the minimum value required by the many design guidelines in engineering practices, such as fills for residential development (BD, 2009; GB 51254, 2017) and embankments (AASHTO, 2010). The specimen for the WRC test was prepared in a similar approach, except that the oven-dried soil was mixed with water. The detailed states of both specimens are summarized in Table 1.

For the shearing tests on OS (series II), the oven-dried soil was mixed with oil to different gravimetric oil contents of 16.9%, 13.7%, 12.2% and 11.0%. Similar to the ORC test, the mixture was statically compacted into the shear box with a target dry density of 1.75 g/cm^3. The resultant degrees of oil saturation are 100%, 81%, 72% and 65%. The specimens in a fully saturated state were obtained from initial specimens with a 72% degree of saturation. Prior to achieving full saturation, these specimens underwent a 24-hour pre-soaking process within a shear box. A similar method was used to prepare WS for the direct shear tests in series III. The degrees of liquid saturation were kept the same between series II and series III.

2.3. Test apparatuses

As shown in Figure 3a, the pressure plate was used to investigate the oil and water retention behaviour. For the measurement of ORC, the high air entry value ceramic disk (i.e., 5.0 and 1.4 bars under the water-saturated and oil-saturated conditions, respectively) in the pressure plate was saturated by oil. During testing, the air pressure (u_a) inside the pressure plate was controlled while the oil

pressure (u_o) beneath the ceramic disk was maintained at atmospheric conditions. It is, therefore, that the air-oil suction (u_a - u_o) of the air-oil interface was applied to the specimen based on the axis translation technique (Hilf, 1956). In addition, the oil flowing in/out of the specimen is recorded through the oil level mark of a ballast tube. The measurement of WRC is similar to that of ORC, except that the high air entry value ceramic disk is saturated by water. During testing, the water pressure (u_w) beneath the ceramic disk remains atmospheric. The suction produced by the air-water interface (u_a - u_w) is controlled by altering the air pressure inside the pressure plate (u_a).

The direct shear apparatus was used to study the shear behaviour of OS and WS. As shown in Figure 3b, the shearing rate is controlled by a stepper motor drive, and the normal stress is applied to the specimen by a loading rod. During testing, the horizontal and vertical displacements are measured through two linear variable differential transformers (LVDTs) and the shear forces are recorded by a dynamometer equipped with an LVDT. All the sensors were connected to a datalog to achieve an automatic data collection with an interval of 25 seconds.

2.4. Test procedures

The ORC and WRC were both determined along the wetting process. Starting from the as-compacted condition, soil suction was decreased stepwise. The cut-off criterion of each step was based on the changing rate of gravimetric liquid content (less than 0.04% per day). During the wetting process, the oil/water infiltration was monitored to determine the equilibrium degree of oil/water saturation at each suction condition.

The direct shear test was conducted following the procedures in ASTM D6528 -17 (ASTM 2017b). Each specimen was set up in the shear box and the shear box was covered by plastic wrap to prevent the evaporation of pore liquid. The calibration test on the impact of the plastic wrap on the measured strength values was conducted and the impacted strength values are less than 1.3 kPa, which is closely approximating the friction value of the apparatus. Suction measurements were not taken during the test. However, based on subsequent measurements and retention curves, it was determined

that the variation in suction did not exceed 5 kPa in WS and 1 kPa in OS. In the initial stage of the test, the predefined normal stress (i.e., 50, 100, 200 and 400 kPa) was applied for consolidation. After that, the specimen was sheared under a constant rate of 0.005 mm/min. Based on some trial tests, the measured stress-displacement relationship and shearing-induced deformation are independent of the shearing rate when it is below 0.005 mm/min. Note that the saturated specimens were sheared under the drained condition, while the undrained condition was designed for the unsaturated specimens. Although the long-term effects of organic fluid on soil have been investigated by Izdebska-Mucha and Trzciński (2021) that the long-term impact of petroleum fuels resulted in the reduction of the zeta potential and repulsive forces between the clay particles, the potential long-term effects were deemed negligible in this study since the tests were conducted just one day after specimen preparation.

SEM tests were carried out using the JSM-7100F (Japan Electron Optics Laboratory Corporation LTD., Japan). Small cubic specimens (about 5 mm × 5 mm × 5 mm) were prepared for the SEM. The small cubic specimens were immersed in liquid nitrogen and immediately put into the freeze-dryer chamber for 48 hours to remove the frozen liquid inside the soil pores. The above specimen preparation method proved effective in protecting soil microstructure (Delage et al., 1996).

3. Interpretations of experimental results

3.1. Microstructures of OS and WS

Figure 4 shows the SEM images of OS and WS. For each specimen, two magnifications (i.e., 1000x and 2000x) are presented. In the small-magnification image of OS (Figure 4a), aggregates with a radius of a few tens of micrometers are identified. The pores between these aggregates are termed inter-aggregate pores. The enlargement of this image (Figure 4b) shows more clearly aggregates which are formed by clay and silt particles. In addition, the intra-aggregate pores are visible. Similar aggregated structures of oil-contaminated soils were reported by previous studies (Nasehi et al., 2016; Khosravi et al., 2013). For WS (Figures 4c and 4d), the microstructure is quite different from that of

OS. The aggregates and dual pore structure failed to be identified in WS. The clay particles in WS tend to envelop the silt particles and fill the intergranular voids.

Although the particle size distributions of OS and WS are the same, SEM images demonstrate that the former and latter specimens are characterized as aggregated and matrix structures (Delage et al., 1996), respectively. The observed variations can be attributed to multiple factors, with the wettability of soil particles towards oil and water being the primary consideration. For WS, the clay volume is enlarged due to hydration (e.g., interstratified illite/montmorillonite), which tends to induce clay paste surrounding the silt particles (Delage et al., 1996). The compaction effort is dispelled in the plastic deformation of a clay paste containing silt particles. For OS, the particles conserve their shapes due to the low wettability of soil particles to oil. During compaction, the resistant aggregates originally formed in oven-dried and sieved powder are difficult to erase (Tarantino, 2010; Romero et al., 2011). Furthermore, the nonpolar nature of silicone oil does not facilitate the development of a double layer, as observed with water and clay (Olson and Mesri, 1970; Chen et al., 2000). Consequently, the formation of a clay paste is more challenging with silicone oil, resulting in distinct structural differences when compared to WS conditions. Additionally, the higher viscosity of silicone oil (5 cst) compared to water (1 cst) leads to a more densely packed structure in OS samples (Ratnaweera and Meegoda, 2006). Moreover, the absence of a double layer in nonpolar fluids highlights the dominance of van der Waals attractive forces as the primary physico-chemical factor (Chen et al., 2000). The lower dielectric constant of silicone oil (approximately 2.7, compared to water's value of 80) further enhances attractive forces between particles in OS (Kaya and Fang, 2000), resulting in a more aggregated structure.

3.2. Silicone oil and water retention curves

Figure 5 shows the results of ORC and WRC along the wetting process. For the ORC, the degree of oil saturation increases (slope: 28.6 (log kPa)$^{-1}$) with decreasing suctions until the 100% degree of saturation is reached at a suction of 0.1 kPa. For the WRC, the adsorption rate is 26.6 (log kPa)$^{-1}$, which is similar to that in the ORC. The WRC reaches a 100% degree of saturation at a larger suction (about 3.0 kPa) than the ORC, demonstrating that the soil has a lower retention capacity for oil than that for water. This is partially because the interfacial tension of air-water (i.e., 72 dynes/cm at 25 °C) is 265% larger than that of air-oil (i.e., 19.7 dynes/cm at 25 °C, XIAMETER™ PMX-200 Silicone Fluid).

The scaling concept is widely used to model the liquid retention behaviour. The retention curve of any liquid is predicted from the WRC by applying a scaling factor (Anderson, 1987; Gee et al., 1991). The advantage of the scaling concept is that the retention curves of different liquids can be described in a unified pattern with a few parameters. In this study, the ORC and WRC are described with the scaling concept together with the v-G equation (van Genuchten, 1980) as follows:

$$S_{r,l} = \frac{1}{(1+(a\beta s_{aw})^{n})^{m}} \tag{1}$$

where $S_{r,l}$ is the degree of liquid saturation; s_{aw} is the suction produced by the air-water interface; β is the scaling factor; a, n and m are soil parameters. According to previous studies of sand (Parker et al., 1987; Goel and O'Carroll, 2011), the scaling factor β can be estimated by the ratio of interfacial tension (i.e., $\beta=T_{al}/T_{aw}$, where T_{aw} and T_{al} are interfacial tensions of air-water and the air-scaled liquid respectively). This equation was verified using the ORCs and WRCs of several sands by previous researchers, but not using test data of other soils.

Equation (1) is used to analyze the results in Figure 5. In the analysis of the WRC, β was 1, and the other parameters were calibrated through the least-square fitting: a=0.0705; n=1.5129 and m=0.1594. Then, these parameters are used to calculate the WRC. As shown by the comparisons between measured and calculated WRCs, the equation has a good performance with a high value of R^2 (i.e., 0.99). Regarding the analysis of the ORC, the scaling factor β was estimated to be 0.274 based

on the interfacial tensions of air-oil and air-water interfaces. With the estimated β value, the ORC is calculated and shown in Figure 5 for comparison (i.e., ORC-II). It is obvious that the calculated ORC significantly overestimates the oil retention capacity. This is because, apart from the difference in interfacial tension, WS and OS have different microstructures, as shown in Figure 4. WS is expected to have a higher retention capacity than OS because of larger inter-aggregate pores in the latter specimen. WS and OS contain electrically contrasting pore fluids (i.e., water and silicone oil). Following Jang and Santamarina (2016), the fluid chemistry-dependent particle interactions could be evaluated by the electrical sensitivity (*SE*):

$$SE = \sqrt{\left[\frac{LL_{DW}}{LL_{brine}}(1 - c_{brine}LL_{brine}) - 1\right]^2 + \left[\frac{LL_{\text{ker}}}{LL_{brine}}\left(\frac{1 - c_{brine}LL_{brine}}{G_{\text{ker}}}\right) - 1\right]^2} \quad (2)$$

where LL_{DW}, LL_{brine}, and LL_{ker} are the liquid limits of soil with deionized water, 2-M NaCl brine and kerosene, respectively; c_{brine} is the concentration of NaCl brine (g/g); G_{ker} is the ratio of the unit weight of kerosene to that of water. Based on the liquid limits of CDG soil with deionized water (i.e., LL_{DW} = 32), 2-M NaCl brine (i.e., LL_{brine} = 30), and kerosene (LL_{ker} = 43), the electrical sensitivity of the CDG soil is equal to 0.61. The CDG soil is classified as the low-plasticity soil of intermediate electrical sensitivity (Jang and Santamarina, 2016), in which the van der Waals and double-layer effects could have an impact. The overestimation of ORC using the parameters of WRC and scaling theory probably can also be explained by the stronger interactions between water and particle than oil-particle interactions. To further analyze the ORC using equation (1), an alternative approach was used. Keeping the parameters obtained from WRC (i.e., a=0.0705; n=1.5129 and m=0.1594) constant, β was determined by fitting the ORC using equation (1): β = 0.018. The calculated ORC is shown in Figure 5 as the solid line (i.e., ORC-II). The calculated and measured ORCs are quite consistent (R^2=0.97), suggesting that the scaling concept could still be used to estimate the ORC from the WRC. However,

the scaling factor should be determined with great caution and not simply assumed to be a ratio of interfacial tensions.

Based on the retention curves, the oil/water contents employed in the direct shear test (65 ~ 100%) suggest that the air-oil suction ranges from 0 to 2 kPa, while the air-water suction ranges from 0 to 30 kPa. Due to the substantially higher suction range of WS compared to OS (i.e., more than tenfold), the suction effects are expected to be more significant in WS than those in OS.

3.3. Stress-strain relationship and deformation behaviour

Figure 6a shows the relationships between shear stress and horizontal displacement of OS under the normal stress of 50 kPa. A strain-softening behaviour is consistently observed for all saturated and unsaturated specimens. With increasing horizontal displacement, the shear stress first increases almost linearly at the initial state, reaches the peak value at about 1.0 mm, and then decreases until a residual shear stress. Figure 6b shows the corresponding vertical displacement induced by shearing. All specimens dilate with increasing horizontal displacement, which is consistent with the strain-softening pattern of stress-displacement curves. Moreover, no significant difference is observed for the stress-displacement curves and shearing-induced vertical displacements at different degrees of oil saturation.

Figures 6c to 6h show the shear behaviour of OS under net normal stresses of 100, 200 and 400 kPa. Again, the influence of oil content on the shear behaviour is negligible. At a given degree of oil saturation, the stress-displacement curves change from strain-softening to strain-hardening with increasing net normal stress, accompanied by less dilation. This is because the over-consolidation ratio of OS decreases with increasing net normal stress.

The results of WS are shown in Figure 7. Similar to the behaviour of OS, WS at lower stress shows stronger strain-softening and larger dilation at a given degree of saturation. More importantly, Figure 7 shows an obvious influence of water content on the shear behaviour. At a given net normal stress, the specimens change from strain-hardening to strain-softening with a decreasing degree of water saturation.

3.4. Shear strength at the residual state

The following equation can describe the shear strength characteristics of a cohesionless soils:

$$\tau_f = c_t + \sigma \tan \phi' \quad (3)$$

where τ_f is the shear strength; c_t is the total cohesion, which is the sum of effective cohesion and apparent cohesion (suction-induced cohesion). Figure 8a shows the relationships between net normal stress and residual shear strength of OS at different degrees of oil saturation. The residual shear strength in each test was determined by taking the average shear stresses when the shear displacement was from 7.0 to 8.0 mm. At 100% degree of oil saturation, the residual shear strengths were fitted using equation (3) with zero total cohesion. At 81%, 72% and 65% degrees of oil saturation, the residual shear strengths were fitted using the same equation with a fixed friction angle equaling that at saturated conditions. All failure envelopes are well captured with high values of R^2 (i.e., larger than 0.99). Within the saturated condition, it is observed that the effective friction angle of OS specimens (44.4°) surpasses that of WS specimens (34.2°). It is commonly understood that oil tends to coat soil particles, acting as a lubricant and consequently reducing the friction angle and bearing capacity of soil (Dai et al., 2016; Kererat, 2019). Conversely, the shear strength of soil typically decreases with an increase in fluid viscosity (Ratnaweera and Meegoda, 2006). Hence, additional factors must contribute significantly to the increased effective friction angle observed in OS. As previously mentioned, the lower dielectric constant of silicone oil compared to water results in a higher net attractive force between particles in OS (Chen et al., 2000). This leads to enhanced shearing resistance at interparticle contacts and, consequently, a larger friction angle in OS. Extrapolating from these results, it can be inferred that the dielectric constant and the influence of van der Waals attractive forces exert a more dominant impact in saturated conditions when comparing OS and WS specimens.

Furthermore, the failure envelopes of OS are insensitive to the degree of oil saturation. The air-oil suction is expected to strengthen the soil skeleton because of the negative pore oil pressure and the capillary force in the liquid meniscus (Wheeler et al., 2003; Ng et al., 2020). Based the low air-oil

suction range (i.e., less than 2 kPa), the suction-induced skeleton hardening is expected to be insignificant for OS tested in this study. Note that the above results are different from previous studies showing that the shear strength and friction angle of OS decreases with increasing the oil content (e.g., Al-Sanad et al., 1995; Puri, 2000). This is probably due to the different oil type in this study and the previous studies.

Figure 8b shows the relationships between net normal stress and residual shear strength of WS at different degrees of water saturation. The methods of determining the residual shear strengths and fitting the failure envelopes are the same as those for OS. As shown in Table 4, the residual friction angle of WS is equal to 34.2^{o}. Based on triaxial compression tests, the CDG soils in Hong Kong usually have friction angles ranging from 33^{o} to 39^{o} (e.g., Fredlund and Rahardjo, 1993; Chen et al., 2004; Ng and Chiu, 2003; Zhang et al., 2008). The friction angle of WS measured in this study is reasonable compared to those measured in previous studies. The residual friction angle of OS (i.e., 44.4^{o}) is about 30% larger than that of WS (i.e., 34.2^{o}). This can also be explained using the aggregated structure of the former specimen, which includes more particle contacts. Furthermore, the apparent cohesion of WS increases from zero to 34.3 kPa as the degree of water saturation decreases from 100% to 65%, different from the behaviour of OS. As shown in Figure 5, the suction of WS increases from zero to around 30 kPa with decreasing the degree of water saturation from 100% to 65%, which could induce more pronounced skeleton hardening than OS.

In addition, it should be noted that the soil's mineralogical composition has a significant influence on its shearing behaviour, including factors such as the residual friction angle and undrained shear strength. This has been demonstrated in studies investigating the behaviour of various clay minerals mixed with water (Trauner et al., 2005; Tiwari and Marui, 2005). It can be inferred that the interaction between silicone oil and different clay minerals would also have diverse impacts on the shear strength of the soil. However, considering the vast number of possible combinations of mineral compositions and organic fluid types, it is important to acknowledge that clear conclusions regarding the

mineralogical composition cannot be drawn solely from the experiments conducted in this study.

3.5. Total cohesions

Figure 9 shows the measured total apparent cohesions of OS and WS. The measured apparent cohesions are the interceptions of failure envelopes representing zero normal stress, as shown in Table 4. The total cohesions of OS specimens are all less than 5 kPa, while WS demonstrates an increasing trend, reaching 35 kPa as the degree of water saturation decreases from 100% to 65%. These observed different trends are attributed to the higher suction range in WS compared to that in OS. However, due to the apparatus limitation (not suction controlled), the parameter κ cannot be calculated without measured degree of liquid saturation and suction. In future studies, utilizing a suction-controlled apparatus to conduct a more comprehensive investigation of oil-contaminated soil within the framework of unsaturated soil mechanics is necessary.

4. Summary and conclusions

This study aimed to investigate the shear behaviour of CDG soil with varying silicone oil contents through a series of direct shear tests. A novel approach was employed, wherein the oil retention curve (ORC) was measured using the pressure plate test, enabling the exploration of the effects of oil retention ability on the shear behaviour of oil-contaminated soil. Water-filled specimens were also tested to serve as a benchmark for the oil-contaminated specimens. Microstructure analysis was conducted using Scanning Electron Microscope (SEM) test on both OS and WS specimens to explore the differences in soil structures. The following key conclusions were drawn from the study:

(1) Microstructure analysis revealed that OS and WS exhibit aggregated and matrix structures, respectively. The aggregated structure of OS is characterized by a higher number of particle contacts and interlocking compared to the matrix structure of WS. These structural differences can be attributed to varying fluid properties, such as wettability, viscosity, and dielectric constant.

(2) The retention capacity of silt for silicone oil is smaller compared to water, primarily due to the lower interfacial tension at the air-oil interface and the aggregated structure exhibited by OS. The

scaling concept can be employed to unify the modelling of WRC and ORC. However, assuming a scaling factor based solely on the ratio of interfacial tensions may lead to an overestimation of oil retention capacity, likely resulting from weaker oil-particle interactions compared to water-particle interactions.

(3) The friction angle of OS is approximately 30% larger than that of WS, primarily attributable to the greater net van der Waals attractive force and the more aggregated structure exhibited by OS, resulting in increased shearing resistance. The failure envelopes of OS were found to be insensitive to the degree of oil saturation. According to the ORC results, the suction range observed in OS at oil saturation degrees between 65% and 100% were all negligible, measuring less than 2 kPa. Consequently, suction-induced skeleton hardening was deemed insignificant for the OS specimens tested, which is illustrated by the pronounced lower total cohesion of OS than that of WS.

Data Availability Statement

Some or all data, models, or codes that support the findings of this study are available from the corresponding author upon reasonable request.

Acknowledgement

This work is supported by the Research Grants Council (RGC) of the HKSAR through the research grant 16204817. The authors also would like to thank the National Science Foundation of China (52022004 and 52279109) and the Technology Innovation Center for Land Engineering and Human Settlements, Shaanxi Land Engineering Construction Group Co., Ltd and Xi'an Jiaotong University (201912131-A1).

References

AASHTO (2010). Standard method of test for moisture-density relations of soils using a 2.5-kg (5.5-lb) rammer and a 305-mm (12-in.) drop. AASHTO standard T99-10. American Association of State and Highway Transportation Officials (AASHTO), Washington, D.C.

Al-Sanad, H. A., Eid, W. K., and Ismael, N. F. (1995). Geotechnical properties of oil-contaminated

Kuwaiti sand. Journal of Geotechnical Engineering, 121(5), 407-412.

Anderson, W. (1986). Wettability literature survey-part 2: Wettability measurement. Journal of Petroleum Technology, 38(11), 1246-1262.

ASTM. (2017a). "Standard test methods for liquid limit, plastic limit, and plasticity index of soils." ASTM D4318, American Society for Testing and Materials, West Conshohocken, Pa.

ASTM. (2017b). "Standard test method for consolidated undrained direct simple shear testing of fine grain soils." ASTM D6528, American Society for Testing and Materials, West Conshohocken, Pa.

ASTM. (2012). "Standard test methods for laboratory compaction characteristics of soil using standard effort." ASTM D698, American Society for Testing and Materials, West Conshohocken, Pa.

ASTM. (2017c). "Standard test methods for particle-size distribution (gradation) of soils using sieve analysis." ASTM D6913/D6913M, American Society for Testing and Materials, West Conshohocken, PA.

ASTM. (2017d). "Standard test method for particle-size distribution (gradation) of fine-grained soils using the sedimentation (hydrometer) analysis." ASTM D7928, American Society for Testing and Materials, West Conshohocken, PA.

Buildings Department (BD). (2009). Practice Note for Authorised Persons and Registered Structural Engineers APP 15, 55, Site Formation - Temporary or Permanent Filling Work, Hong Kong Special Administrative Region Government, Hong Kong.

Chen, J., Anandarajah, A. & Inyang, H. (2000) Pore fluid properties and compressibility of kaolinite. Journal of geotechnical and geoenvironmental engineering 126(9):798-807.

Chen, H., Lee, C. F., and Law, K. T. (2004). Causative mechanisms of rainfall-induced fill slope failures. Journal of Geotechnical and Geoenvironmental Engineering, 130(6), 593-602.

Cui, Y., Delage, P., and Alzoghbi, P. (2003). Retention and transport of a hydrocarbon in a silt. Géotechnique, 53(1), 83-91.

Dai, B. B., Yang, J. & Zhou, C. Y. (2016) Observed effects of interparticle friction and particle size on

shear behavior of granular materials. International journal of geomechanics 16(1):04015011.

Delage, P., Audiguier, M., Cui, Y. J., and Howat, M. D. (1996). Microstructure of a compacted silt. Canadian Geotechnical Journal, 33(1), 150-158.

Fredlund, D. G., Morgenstern, N. R., and Widger, R. A. (1978). The shear strength of unsaturated soils. Canadian Geotechnical Journal, 15(3), 313-321.

Fredlund, D. G., and Rahardjo, H. (1993). Soil mechanics for unsaturated soils. John Wiley & Sons.

GB 51254 (2017). Technical code for deep filled ground. China Architecture & Building Press Beijing. (in Chinese)

Gee, G. W., Kincaid, C. T., Lenhard, R. J., and Simmons, C. S. (1991). Recent studies of flow and transport in the vadose zone. Reviews of Geophysics, 29(S1), 227-239.

Ghadyani, M., Hamidi, A., and Hatambeigi, M. (2019). Triaxial shear behaviour of oil-contaminated clays. European Journal of Environmental and Civil Engineering, 23(1), 112-135.

Goel, G., and O'Carroll, D. M. (2011). Experimental investigation of nonequilibrium capillarity effects: Fluid viscosity effects. Water Resources Research, 47, W09507.

Han, Z., and Vanapalli, S. K. (2016). Stiffness and shear strength of unsaturated soils in relation to soil-water characteristic curve. Géotechnique, 66(8), 627-647.

Hilf, J. W. (1956). An investigation of pore-water pressure in compacted cohesive soils, PhD Thesis, Technical Memorandum. No. 654, U.S. Department of the Interior, Bureau of Reclamation, Design and Construction Division, Denver, CO.

Hossain, M. A., and Yin, J. H. (2010a). Behaviour of a compacted completely decomposed granite soil from suction controlled direct shear tests. Journal of Geotechnical and Geoenvironmental Engineering, 136(1), 189-198.

Ijaz, N., Ur Rehman, Z. & Ijaz, Z. (2022a) Recycling of paper/wood industry waste for hydromechanical stability of expansive soils: A novel approach. Journal of Cleaner Production 348:131345.

Ijaz, N., Ye, W., Ur Rehman, Z., Dai, F. & Ijaz, Z. (2022b) Numerical study on stability of lignosulphonate-based stabilized surficial layer of unsaturated expansive soil slope considering hydro-mechanical effect. Transportation Geotechnics 32:100697.

Izdebska-Mucha, D. and J. Trzciński (2021). Clay soil behaviour due to long-term contamination by liquid petroleum fuels: microstructure and geotechnical properties. Bulletin of Engineering Geology and the Environment 80: 3193-3206.

Jang, J., and Carlos Santamarina, J. (2016). Fines classification based on sensitivity to pore-fluid chemistry. Journal of Geotechnical and Geoenvironmental Engineering, 142(4), 06015018.

Jia, Y., et al. (2011). The influence of oil contamination on the geotechnical properties of coastal sediments in the Yellow River Delta, China. Bulletin of Engineering Geology and the Environment 70: 517-525.

Kaya, A. & Fang, H.-Y. (2000) The effects of organic fluids on physicochemical parameters of fine-grained soils. Canadian Geotechnical Journal 37(5):943-950.

Kererat, C. (2019) Effect of oil-contamination and water saturation on the bearing capacity and shear strength parameters of silty sandy soil. Engineering Geology 257:105138.

Kermani, M., and Ebadi, T. (2012). The effect of oil contamination on the geotechnical properties of fine-grained soils. Soil and Sediment Contamination: An International Journal, 21(5), 655-671.

Khamehchiyan, M., Charkhabi, A. H., and Tajik, M. (2007). Effects of crude oil contamination on geotechnical properties of clayey and sandy soils. Engineering Geology, 89(3-4), 220-229.

Khosravi, E., Ghasemzadeh, H., Sabour, M. R., and Yazdani, H. (2013). Geotechnical properties of gas oil-contaminated kaolinite. Engineering geology, 166, 11-16.

Mitchell, J. K., and Soga, K. (2005). Fundamentals of soil behaviour (Vol. 3). John Wiley & Sons New York.

Moore, C. & Mitchell, J. (1974) Electromagnetic forces and soil strength. *Géotechnique* 24(4):627-640.

Nasehi, S. A., Uromeihy, A., Nikudel, M. R., and Morsali, A. (2016). Influence of gas oil contamination on geotechnical properties of fine and coarse-grained soils. Geotechnical and Geological Engineering, 34(1), 333-345.

Nasr, A. M. (2009). Experimental and theoretical studies for the behaviour of strip footing on oil-contaminated sand. Journal of Geotechnical and Geoenvironmental Engineering, 135(12), 1814-1822.

Nasr, A. M. (2013). Uplift behaviour of vertical piles embedded in oil-contaminated sand. Journal of Geotechnical and Geoenvironmental Engineering, 139(1), 162-174.

Nasr, A., and Krishna Rao, S. (2016). Behaviour of laterally loaded pile groups embedded in oil-contaminated sand. Géotechnique, 66(1), 58-70.

Ng, C. W. W., and Chiu, A. C. F. (2003). Laboratory study of loose saturated and unsaturated decomposed granitic soil. Journal of Geotechnical and Geoenvironmental Engineering, ASCE, 129(6), 550–559.

Ng, C. W. W., and Menzies, B. (2007). Advanced Unsaturated Soil Mechanics and Engineering. CRC Press.

Ng, C. W. W., Sadeghi, H., and Jafarzadeh, F. (2017). Compression and shear strength characteristics of compacted loess at high suctions. Canadian Geotechnical Journal, 54(5), 690-699.

Ng, C. W. W., Zhou, C., and Chiu, C. F. (2020). Constitutive modelling of state-dependent behaviour of unsaturated soils: an overview. Acta Geotechnica, 15(10), 2705-2725.

Olson, R. E. & Mesri, G. (1970) Mechanisms controlling compressibility of clays. Journal of the Soil Mechanics and Foundations Division 96(6):1863-1878.

Parker, J. C., Lenhard, R. J., and Kuppusamy, T. (1987). A parametric model for constitutive properties governing multiphase flow in porous media. Water Resources Research, 23(4), 618-624.

Puri, V. K. (2000). Geotechnical aspects of oil-contaminated sands. Soil and Sediment Contamination, 9(4), 359-374.

Rajabi, H., and Sharifipour, M. (2019). Geotechnical properties of hydrocarbon-contaminated soils: a comprehensive review. Bulletin of Engineering Geology and the Environment, 78(5), 3685-3717.

Ratnaweera, P. & Meegoda, J. N. (2006) Shear strength and stress-strain behavior of contaminated soils. Geotechnical Testing Journal 29(2):133.

Rehman, Z. U., Ijaz, N., Ye, W. & Ijaz, Z. (2023) Design optimization and statistical modeling of recycled waste-based additive for a variety of construction scenarios on heaving ground. Environmental Science and Pollution Research 30(14):39783-39802.

Romero, E., Della Vecchia, G., and Jommi, C. (2011). An insight into the water retention properties of compacted clayey soils. Géotechnique, 61(4), 313-328.

Safehian, H., Rajabi, A. M., and Ghasemzadeh, H. (2018). Effect of diesel-contamination on geotechnical properties of illite soil. Engineering geology, 241, 55-63.

Sheng, D., Zhou, A., and Fredlund, D. G. (2011). Shear strength criteria for unsaturated soils. Geotechnical and Geological Engineering, 29(2), 145-159.

Sherif, M. A. & Burrous, C. M. (1969) Temperature effects on the unconfined shear strength of saturated, cohesive soil. Effects of Temperature and Heat on Engineering Behavior of Soils, Special report 103:267-272.

Shin, E. C., and Das, B. M. (2001). Bearing capacity of unsaturated oil-contaminated sand. International Journal of Offshore and Polar Engineering, 11(03), 220-227.

Soga, K., Kawabata, J., Kechavarzi, C., Coumoulos, H., and Waduge, W. (2003). Centrifuge modeling of nonaqueous phase liquid movement and entrapment in unsaturated layered soils. Journal of Geotechnical and Geoenvironmental Engineering, 129(2), 173-182.

Tarantino, A. (2010). Unsaturated soils: compacted versus reconstituted states. Proceedings of the 5th International Conference on Unsaturated Soils, Barcelona, Spain, 113-136.

Tiwari, B. & Marui, H. (2005) A new method for the correlation of residual shear strength of the soil with mineralogical composition. Journal of geotechnical and geoenvironmental engineering

131(9):1139-1150.

Trauner, L., Dolinar, B. & Mišič, M. (2005) Relationship between the undrained shear strength, water content, and mineralogical properties of fine-grained soils. International journal of geomechanics 5(4):350-355.

ur Rehman Z, Junaid M F, Ijaz N, et al. Remediation methods of heavy metal contaminated soils from environmental and geotechnical standpoints[J]. Science of The Total Environment, 2023, 867: 161468.

Vanapalli, S. K., Fredlund, D. G., Pufahl, D. E., and Clifton, A. W. (1996). Model for the prediction of shear strength with respect to soil suction. Canadian Geotechnical Journal, 33(3), 379-392.

van Genuchten, M. T. (1980). A closed-form equation for predicting the hydraulic conductivity of unsaturated soils. Soil Science Society of America Journal, 44(5), 892-898.

Wheeler, S. J., Sharma, R. S., and Buisson, M. S. R. (2003). Coupling of hydraulic hysteresis and stress–strain behaviour in unsaturated soils. Géotechnique, 53(1), 41-54.

XIAMETER™ PMX-200 Silicone Fluid, https://www.dow.com/en-us/pdp.xiameter- pmx-200-silicone-fluid-5-cst.01013131z.html?productCatalogFlag=1#properties.

Yu, J. R., Zhou, C., and Mu, Q. Y. (2022). Numerical investigation on LNAPL flow in the vadose zone considering porosity effects on soil hydraulic properties. Vadose Zone Journal, 21(5), e20211.

Zhang, L. M., Xu, Y., and Tang, W. H. (2008). Calibration of models for pile settlement analysis using 64 field load tests. Canadian Geotechnical Journal, 45(1), 59-73.

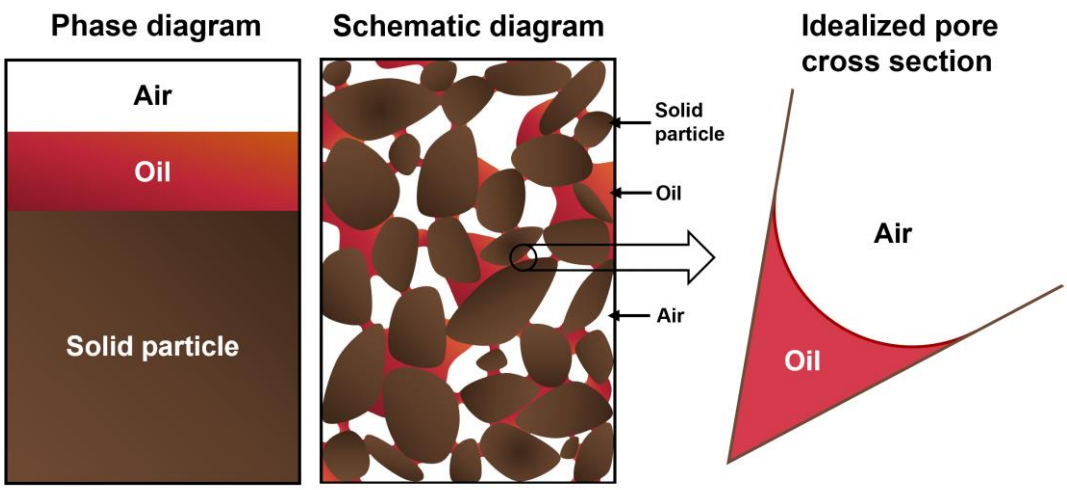

Fig. 1 Schematic diagram of an oil-air-soil three-phase system.

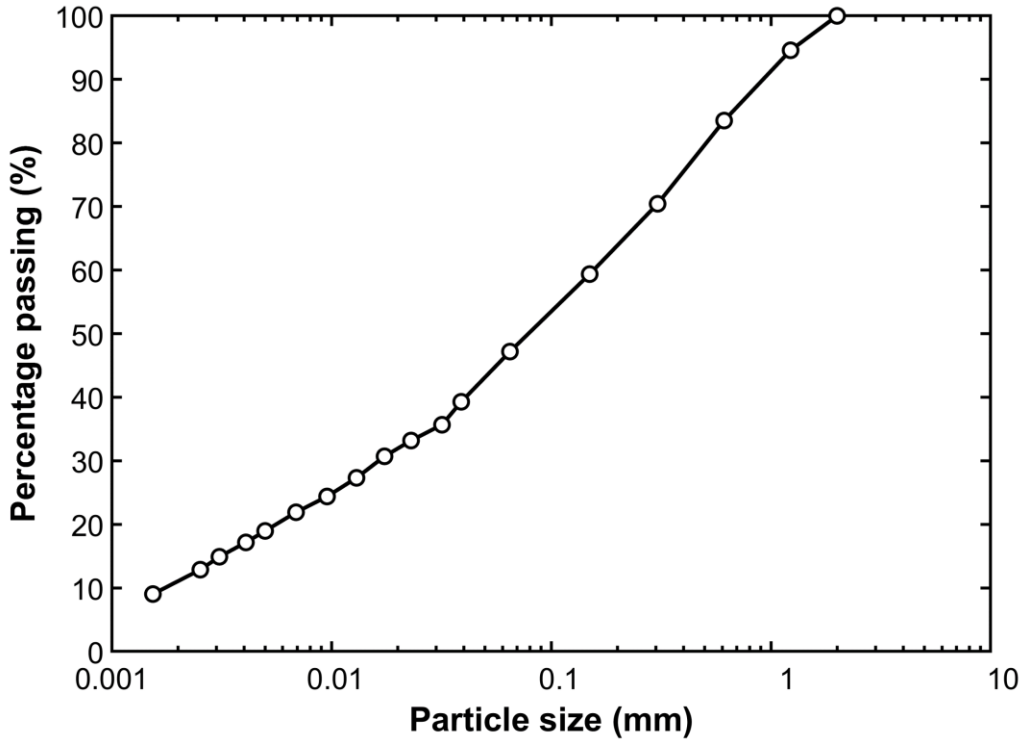

Fig. 2 Particle size distribution of tested soil.

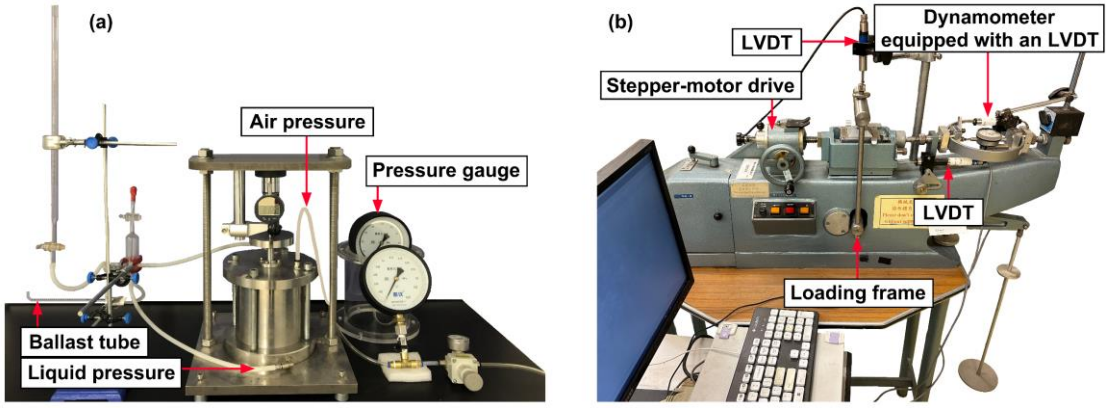

Fig. 3 Photographs of test apparatuses: (a) pressure plate; (b) direct shear.

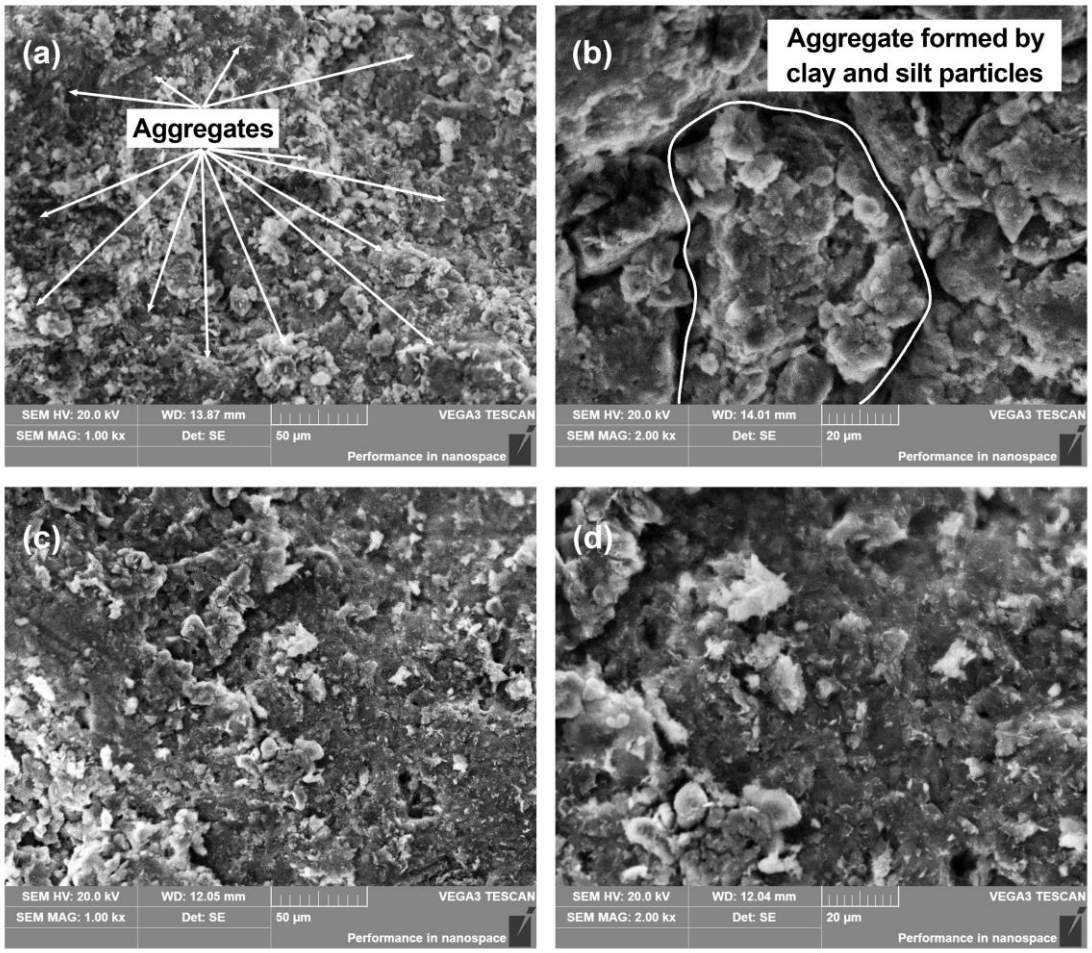

Fig. 4 SEM images of tested specimens: (a) OS 1000 x; (b) OS 2000 x; (c) WS 1000 x; (d) WS 2000x.

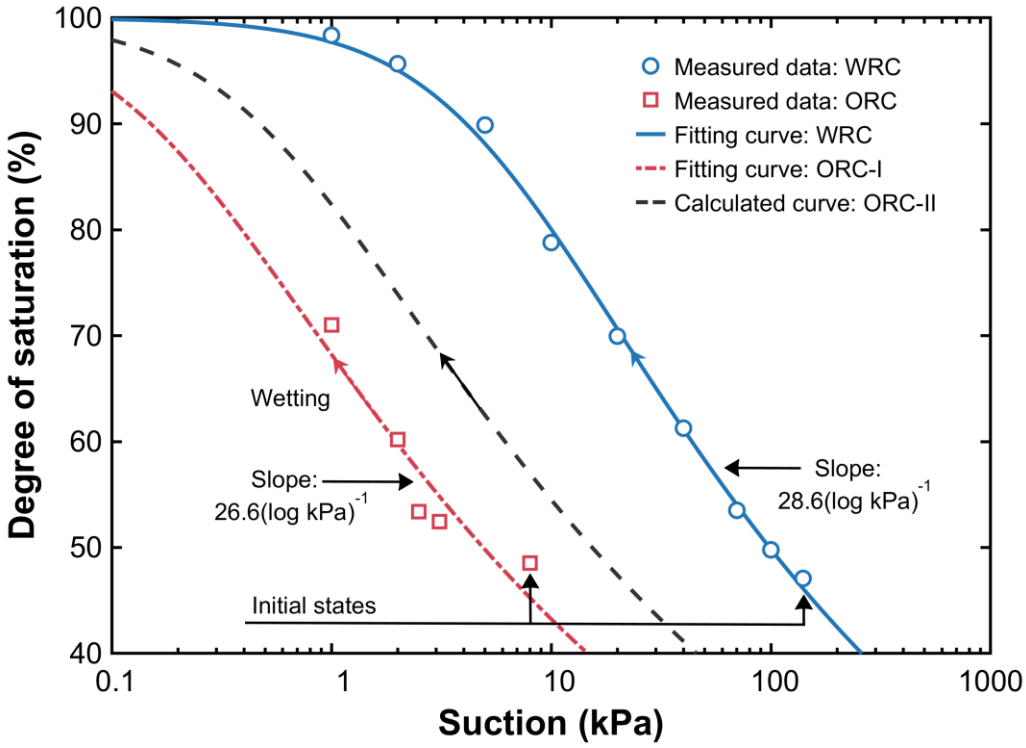

Fig. 5 Water and oil retention curves of tested specimens.

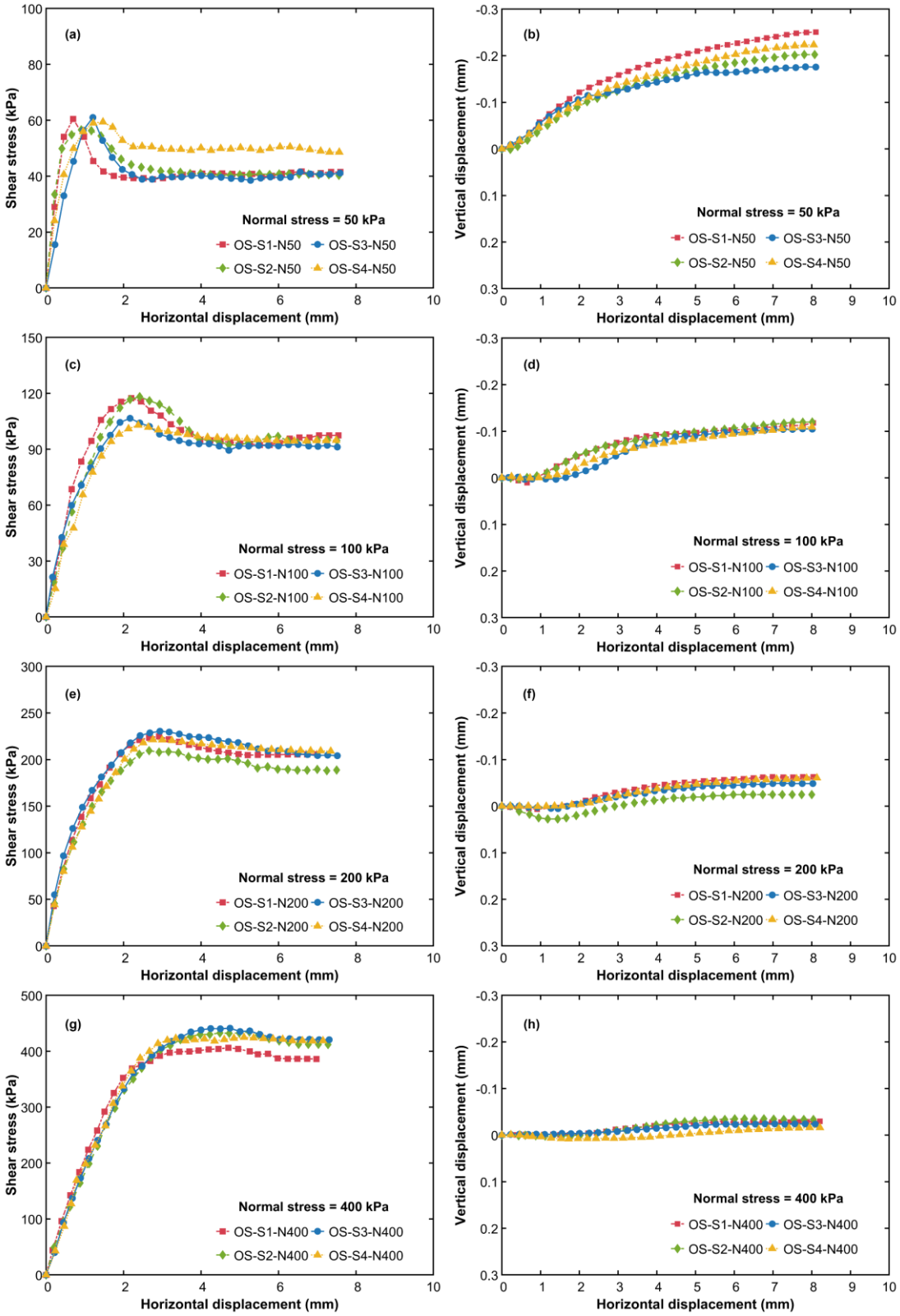

Fig. 6 Shear behaviour of OS under different normal stresses: (a) σ=50 kPa, stress-displacement curve; (b) σ=50 kPa, vertical deformation; (c) σ=100 kPa, stress-displacement curve; (d) σ=100 kPa, vertical deformation; (e) σ=200 kPa, stress-displacement curve; (f) σ=200 kPa, vertical deformation; (g) σ=400 kPa, stress-displacement curve; (h) σ=400 kPa, vertical deformation (positive value: contraction; negative value: dilation).

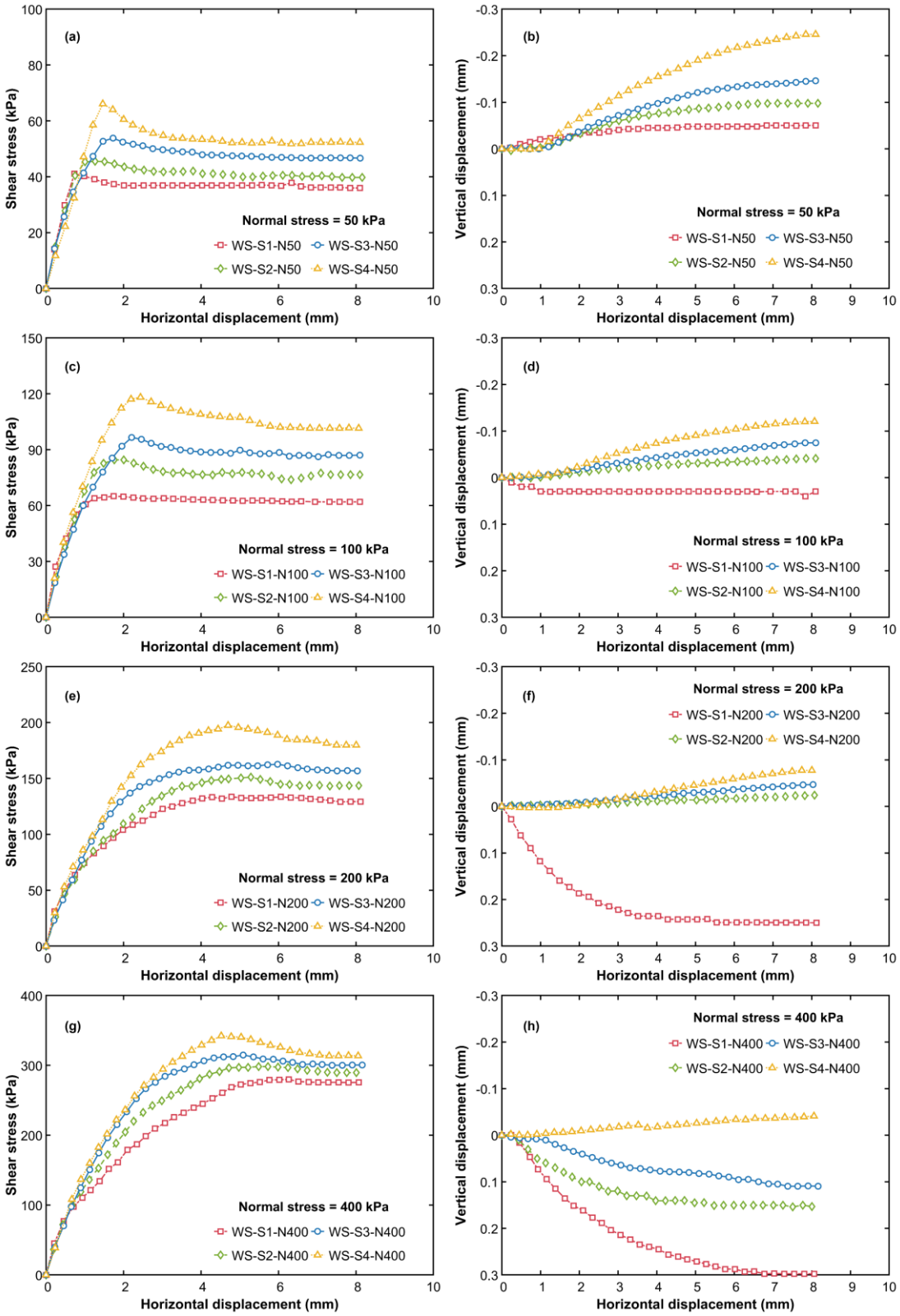

Fig. 7 Shear behaviour of WS under different normal stresses: (a) σ=50 kPa, stress-displacement curve; (b) σ=50 kPa, vertical deformation; (c) σ=100 kPa, stress-displacement curve; (d) σ=100 kPa, vertical deformation; (e) σ=200 kPa, stress-displacement curve; (f) σ=200 kPa, vertical deformation; (g) σ=400 kPa, stress-displacement curve; (h) σ=400 kPa, vertical deformation (positive value: contraction; negative value: dilation).

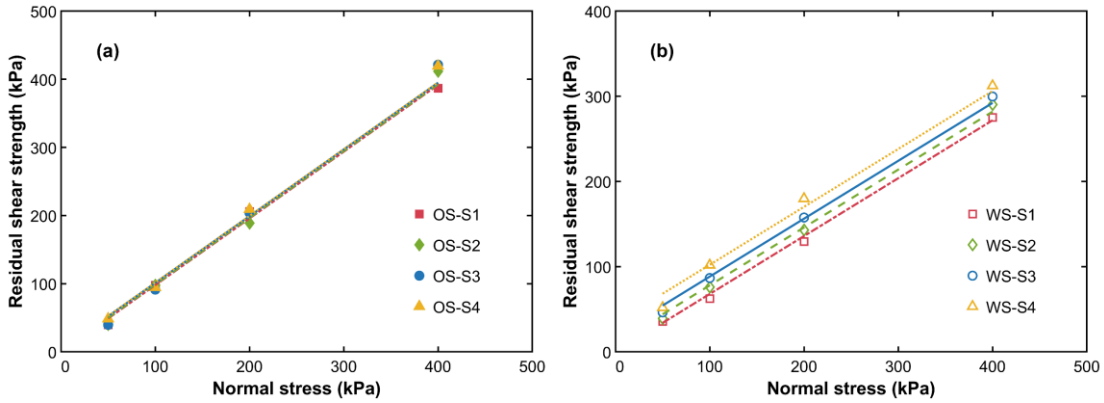

Fig. 8 Failure envelopes represented by residual shear strength: (a) OS; (b) WS.

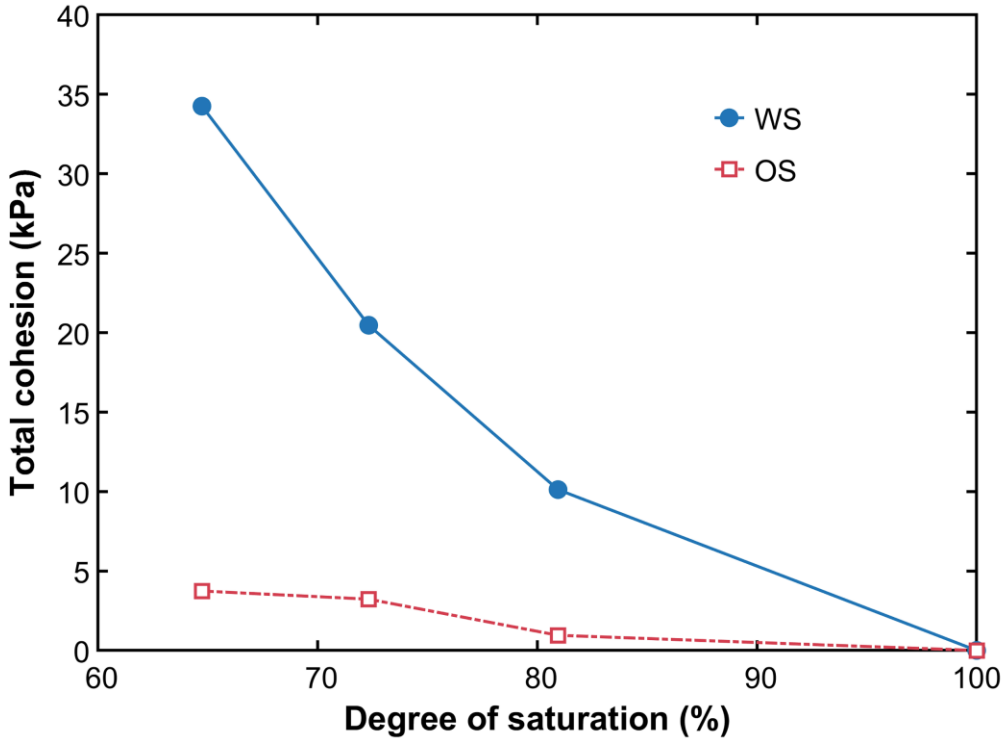

Fig. 9 Total cohesion of OS and WS.

Table 1 Test program and soil states in each test series

Test Series	Specimen ID	Initial state			Normal stress	After compression			After wetting/shearing		
		w (%)	e	Sr (%)	(kPa)	w (%)	e	Sr (%)	w (%)	e	Sr (%)
I	OS	8.4	0.480	50	0	-	-	-	16.9	0.480	100
	WS	8.4	0.480	45	0	-	-	-	18.5	0.480	100
II	OS-S1-N50	16.9	0.480	100	50	16.9	0.480	100	17.6	0.499	100
	OS-S1-N100				100	16.9	0.479	100	17.2	0.488	100
	OS-S1-N200				200	16.8	0.478	100	17.0	0.483	100
	OS-S1-N400				400	16.8	0.477	100	16.9	0.479	100
	OS-S2-N50	13.7	0.480	81	50	13.7	0.480	81	13.7	0.495	79
	OS-S2-N100				100	13.7	0.479	81	13.7	0.488	80
	OS-S2-N200				200	13.7	0.478	81	13.7	0.480	81
	OS-S2-N400				400	13.7	0.477	81	13.7	0.480	81
	OS-S3-N50	12.2	0.480	72	50	12.2	0.480	72	12.2	0.493	70
	OS-S3-N100				100	12.2	0.479	72	12.2	0.487	71
	OS-S3-N200				200	12.2	0.478	72	12.2	0.482	72
	OS-S3-N400				400	12.2	0.477	73	12.2	0.479	72
	OS-S4-N50	11.0	0.480	65	50	11.0	0.480	65	11.0	0.497	63
	OS-S4-N100				100	11.0	0.479	65	11.0	0.487	64
	OS-S4-N200				200	11.0	0.478	65	11.0	0.482	65
	OS-S4-N400				400	11.0	0.477	65	11.0	0.478	65
III	WS-S1-N50	18.5	0.480	100	50	18.5	0.480	100	18.6	0.484	100
	WS-S1-N100				100	18.4	0.479	100	18.4	0.477	100
	WS-S1-N200				200	18.4	0.477	100	17.7	0.459	100
	WS-S1-N400				400	18.3	0.475	100	17.4	0.453	100
	WS-S2-N50	15.0	0.480	81	50	15.0	0.479	81	15.0	0.486	80
	WS-S2-N100				100	15.0	0.479	81	15.0	0.482	81
	WS-S2-N200				200	15.0	0.477	81	15.0	0.479	81
	WS-S2-N400				400	15.0	0.475	82	15.0	0.464	84
	WS-S3-N50	13.4	0.480	72	50	13.4	0.479	72	13.4	0.490	71
	WS-S3-N100				100	13.4	0.479	72	13.4	0.484	72
	WS-S3-N200				200	13.4	0.477	73	13.4	0.480	72
	WS-S3-N400				400	13.4	0.474	73	13.4	0.466	74
	WS-S4-N50	12.0	0.480	65	50	12.0	0.480	65	12.0	0.498	62
	WS-S4-N100				100	12.0	0.479	65	12.0	0.488	64
	WS-S4-N200				200	12.0	0.478	65	12.0	0.484	64
	WS-S4-N400				400	12.0	0.475	65	12.0	0.478	65

Note: w, gravimetric water/oil content; e, void ratio; Sr, degree of water/oil saturation

Table 2 Properties of tested soil

Parameter	Value
Specific gravity	2.59
Liquid limit (%)	32
Plastic limit (%)	21
Plasticity index (%)	11
Maximum dry density (g/cm^3)	1.84
Optimum water content (%)	13.4
Particle size distribution (%)	
Sand (0.075-2 mm, %)	49.1
Silt (0.005-0.075 mm, %)	28.8
Clay ($\leqslant$0.005 mm, %)	22.1

Table 3 Properties of the tested silicone oil (XIAMETER™ PMX-200 Silicone Fluid)

Parameter	Value
Composition	Dimethicone
Dry density at 25℃ (g/cm^3)	0.913
Kinematic viscosity at 25℃ (m^2/s)	5.0×10^{-6}
Surface tension at 25℃ (N/m)	19.7×10^{-3}
Solubility parameter at 25℃ ((J/cm^3)$^{1/2}$)	7.1

Table 4 Failure envelope of OS and WS

Specimens	Failure envelope (residual state)
OS-S1	τ_f = tan44.4° * σ (R^2 = 0.999)
OS-S2	τ_f = tan44.4° * σ + 0.9 (R^2 = 0.993)
OS-S3	τ_f = tan44.4° * σ + 3.2 (R^2 = 0.993)
OS-S4	τ_f = tan44.4° * σ + 3.7 (R^2 = 0.993)
WS-S1	τ_f = tan34.2° * σ (R^2 = 0.998)
WS-S2	τ_f = tan34.2° * σ + 10.1 (R^2 = 0.998)
WS-S3	τ_f = tan34.2° * σ + 20.4 (R^2 = 0.996)
WS-S4	τ_f = tan34.2° * σ + 34.3 (R^2 = 0.991)

1